Investigation of Depth of Interaction Encoding for a Pixelated LSO Array With a Single Multi-Channel PMT

Yongfeng Yang, *Member, IEEE*, Yibao Wu, *Senior Member, IEEE*, and Simon R. Cherry, *Fellow, IEEE*

***Abstract*—A new approach to depth of interaction (DOI) encoding for a pixelated LSO array using a single multi-channel PMT was investigated. In this method the DOI information was estimated by taking advantage of optical crosstalk between LSO elements and examining the standard deviation (spread) of signals on all channels of the PMT. Unpolished and polished 6×6 LSO arrays with a crystal size of $1.3 \times 1.3 \times 20$ mm^3 were evaluated on a Hamamatsu H7546 64-channel PMT. The arrays were placed on the center of the PMT and the central 16 channels of the PMT were individually read out and digitized. For the unpolished array, all crystals were resolved in the flood histogram. An average DOI resolution of 8 mm was obtained. The energy resolution was $\sim$25% after the signal amplitude was corrected using the measured DOI information. For the polished array, the flood histogram was superior to the unpolished array, however no DOI information could be measured. Using unpolished crystals, this method could be a practical way to achieve limited DOI information in PET detectors. The standard deviation of all PMT channels can be readily obtained using a resistor network. Only five signals (four signals to determine the x-y position and one signal measuring the standard deviation) need to be digitized, and this method only requires a single photon detector to read out the array. Unlike phoswich detectors, the method does not require segmenting the scintillator array into layers. The measured DOI resolution was much worse than that obtained with the dual-ended readout method, however, it was similar to that obtained with a two-layer phoswich detector.**

***Index Terms*—Depth of interaction, positron emission tomography (PET), small-animal imaging.**

I. Introduction

RECENT research in positron emission tomography (PET) physics can be divided into two major areas of endeavor. On the clinical side, efforts have been made to improve image quality using time of flight PET [1] and by developing improved algorithms for scatter and attenuation correction, image reconstruction, and motion correction [2], [3]. On the preclinical side, the main focus is to improve the spatial resolution and sensitivity of the PET scanners [4]–[6] as well as to develop multimodality systems that combine PET with magnetic resonance imaging [7]–[10], x-ray computed tomography [11], and optical imaging [12]. In current small animal PET scanners, a compromise between sensitivity and spatial resolution is made due to the depth of interaction (DOI) effect. Typically, much shorter crystals (about 10 mm thick compared to 20–30 mm for a clinical scanner) are used for a small animal PET scanner [13]–[15] and the ring diameter is kept larger than needed (about 15 cm), but still the spatial resolution degrades rapidly as you move away from the center of the field of view, even if advanced reconstruction algorithms that model the crystal penetration are used [16]. DOI effects are the single biggest limitation in improving the resolution/sensitivity trade-off in small-animal PET and similar considerations apply for dedicated high-resolution brain and breast clinical PET scanners. For this reason, much attention in recent years has focused on detector designs with depth-encoding ability. DOI encoding techniques include multi-layer detectors consisting of crystal layers with different scintillation light decay times [17]–[20], with different reflector arrangements [21], [22], and using a position shift of half a crystal for different layers [23]; dual-ended readout of scintillator arrays [24]–[27]; measuring charge collection time differences at the cathode and the anode for semiconductor detectors [28], [29]; and measuring light distribution with a multi-channel photomultiplier tube (PMT) for a continuous crystal scintillator detector [30], [31]. Depth-encoding detectors have the potential to allow a PET scanner to be built with a smaller ring diameter and/or using longer crystals while maintaining spatial resolution.

Smaller ring diameter means higher sensitivity, lower cost and a smaller photon noncollinearity effect. Longer crystals mean higher sensitivity. Thus solving the DOI problem is key to the development of higher performance, lower cost, small-animal PET scanners. To date, many of these DOI approaches are either difficult or expensive to implement, therefore, with the exception of a simple 2-layer phoswich [32], depth-encoding detectors have yet to be routinely incorporated into commercial small-animal PET scanners. Thus, developing simpler DOI methods, and improving the performance and robustness of existing methods, remain a priority.

In our previous work, in which DOI was measured by taking the ratio of signals from position-sensitive avalanche photodiodes (PSAPDs) coupled to both ends of a lutetium oxyorthosilicate (LSO) scintillator array, we noted a strong depth dependence of the crystal location in the flood histogram of each PSAPD for unpolished LSO arrays. These unpolished arrays also gave much better DOI resolution than the polished arrays

Manuscript received September 03, 2008; revised December 11, 2008. Current version published October 07, 2009. This work was supported by NIH under Grant R01 EB006109.

The authors are with the Department of Biomedical Engineering, University of California, Davis, Davis, CA 95616 USA (e-mail: yfyang@ucdavis.edu; ybwu@ucdavis.edu; srcherry@ucdavis.edu).

Color versions of one or more of the figures in this paper are available online at http://ieeexplore.ieee.org.

Digital Object Identifier 10.1109/TNS.2009.2016094

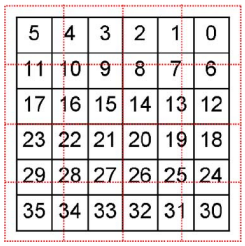

Fig. 1. Relative positions of the LSO crystals on the multi-channel PMT. The solid lines show the 36 crystals of the LSO array. Dashed lines show the central 16 PMT pixels.

[33]. We thought this was in part because the spatial distribution of the light arriving at the photon detector was depth-dependent, caused by depth-dependent leakage of scintillation light across the reflector barrier between LSO elements. If this is true, then it may be possible to extract DOI information by reading out the signal with just one position sensitive photon detector placed at the back of the LSO array. In this paper we introduce this new method of DOI encoding for a pixelated LSO array using a single multi-channel PMT. A similar method has previously been used for DOI encoding of continuous scintillator detectors [30], [31], where the change in light distribution with depth is to be expected based on simple solid angle arguments.

II. Materials and Methods

One unpolished and one polished LSO array were measured in this work. The difference between the two arrays was the surface of the crystals which was left "as cut" or polished during the fabrication of the arrays. Both arrays have 6×6 elements with a crystal size of $1.3 \times 1.3 \times 20$ mm^3. The inter-crystal reflector was the 65 micron-thick Vikuiti™ enhanced specular reflector film (3M, St. Paul, MN) [34]. Details of the array fabrication can be found in [35], [36]. The multi-channel PMT was a Hamamatsu H7546 64-channel PMT with 2 mm square pixels on a 2.3 mm pitch. The arrays were placed on the center of the PMT, and the side of the array opposite to the PMT (the entrance face) was open (no reflector) to maximize the depth dependence of the light distribution on the PMT. The central 16 channels (4×4) of the PMT, which covered the dimensions of the entire LSO array, were read out and individually digitized. The position of the 36 crystals on the PMT pixels is shown in Fig. 1. Standard NIM electronics were used for signal processing. The data acquisition system has been described previously [37].

The gain of the 16 PMT channels was calibrated by uniformly illuminating the PMT with a light-emitting diode (LED) (HLMP-CB26-SV000, Agilent Technologies). Both arrays were measured in singles and coincidence modes. In singles mode, the arrays were uniformly irradiated from one side by a 0.5 mm ^{22}Na point source. In coincidence mode, five depths of 2, 6, 10, 14, and 18 mm from the PMT were selectively irradiated by electronic collimation using a LSO slab detector with a thickness of 2 mm. A detailed description of the electronic collimation method is presented in [36]. The width of the radiation beam at the LSO arrays is estimated from the experimental geometry to be $\sim$2 mm. The flood histogram of the detector was calculated using the 16 PMT signals and the following equations:

80	79	85	85
83	86	74	85
79	100	88	87
78	88	87	80

Fig. 2. Gain of the central 16 channels of the multi-channel PMT. The maximum gain is normalized to a value of 100.

$$x = \sum_{i=0}^{15} A_i \times x_i \tag{1}$$

$$y = \sum_{i=0}^{15} A_i \times y_i \tag{2}$$

where A_i is the signal amplitude measured for the ith PMT channel, and x_i and y_i are the physical x and y coordinates of the ith PMT channel. The DOI was determined using the standard deviation (SD) of the 16 PMT signals with the assumption that events interacting closer to the PMT would have less spread of the scintillation light at the photocathode than those interacting far away. This assumption is based on the fact that the thin polymeric reflectors used in these arrays are not 100% opaque leading to considerable optical crosstalk between crystals, with more crosstalk occurring the further the 511-keV photon interacts from the PMT.

The total energy signal was obtained by summing the 16 PMT signals. There was a significant light loss along the depth for the unpolished array used in this work, therefore, the energy resolution as measured from histogramming the events from a particular crystal is poor. The energy information can be improved by incorporating the measured DOI information to correct for the depth-dependent light collection efficiency. This leads to improved energy resolution and is discussed in more detail in the next section.

III. Results

The relative gain of the 16 PMT channels are shown in Fig. 2. The minimum gain is 74 if the maximum gain is normalized to a value of 100. The standard deviation of the gains of the 16 PMT channels is 7%. Data was analyzed both with and without applying a PMT gain calibration to the measured signals. We found that the gain calibration did not significantly change the appearance of the flood histogram, nor the DOI resolution, probably because the gain variations of 16 channels for the PMT used in this work were relatively small. However, all results shown here were obtained with gain calibration.

The flood histograms from the polished and unpolished arrays obtained at depths of 2, 10, and 18 mm (with respect to the PMT face), and for uniform irradiation of the entire array, are shown in Fig. 3. For the polished array, the locations of the crystals in the flood histograms show very little change with depth. The flood histogram obtained by irradiating at all depths is very

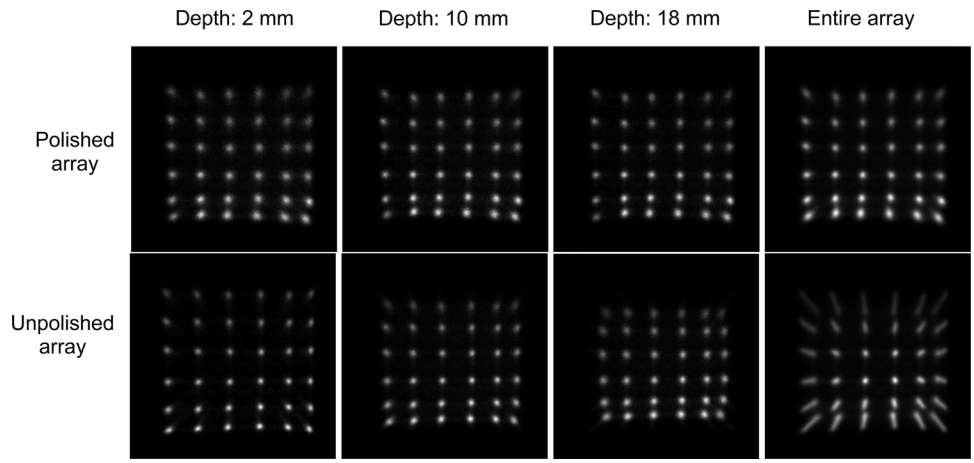

Fig. 3. Flood histograms of polished and unpolished arrays measured at three depths of 2, 10, 18 mm, and for irradiation of the entire array. Note the strong depth dependence of the unpolished array.

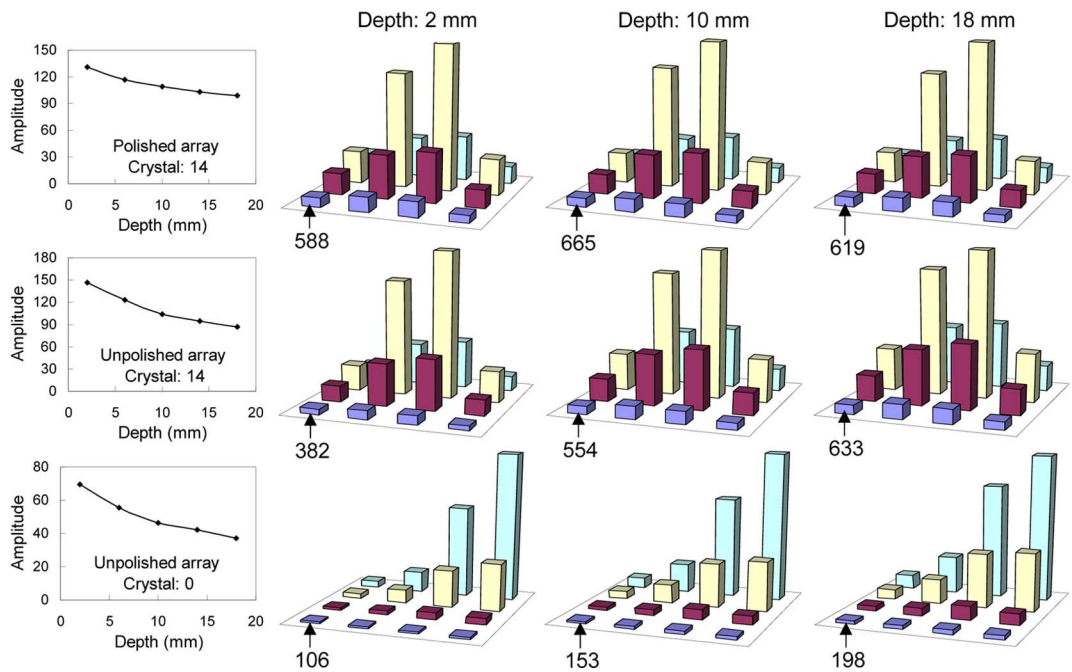

Fig. 4. The photopeak amplitude (relative units) of the total signal (sum of all 16 channels) at different depths and the average light distribution on the 16 PMT channels for individual crystals with irradiation at three depths of 2, 10, and 18 mm from the PMT. The numerical value for one PMT channel is shown to demonstrate the relative magnitude of changes in PMT signals with depth.

good and all the crystals can be clearly resolved. For the unpolished array, the flood histograms are depth-dependent. Two phenomena are observed. 1) The flood histograms degrade as the irradiation depth increases since less light photons reach the PMT cathode at greater depths. 2) The dynamic range of the flood histograms are reduced as the irradiation depth increases since the light cross talk increases. Although the flood histogram for irradiation of the entire array is degraded by the depth-dependent position, it is still possible to resolve all 36 crystals in the array.

Crystal look-up tables were created from the flood histograms of the entire array for both polished and unpolished arrays allowing events to be sorted for each individual crystal. The average light distribution on the 16 PMT channels was obtained for individual crystals by determining the average signal on each of the PMT channels for all events in that crystal. Fig. 4 shows representative results for (a) crystal 14 from the polished array, (b) crystal 14 from the unpolished array and (c) crystal 0 from the unpolished array for irradiation at depths of 2, 10, and 18 mm from the PMT. Crystal 14 is at the center of the array and crystal 0 is a corner crystal (see Fig. 1). The numerical values for the amplitude of one PMT channel (channel 15) also are shown in Fig. 4 to illustrate the relative changes in signal amplitude with depth more clearly. Channel 15 is the bottom left corner channel on the PMT. The amplitude of all channels was normalized so that the maximum amplitude was 10 000. The photopeak amplitude at the 5 different irradiation depths was also obtained from the corresponding energy spectra and is shown

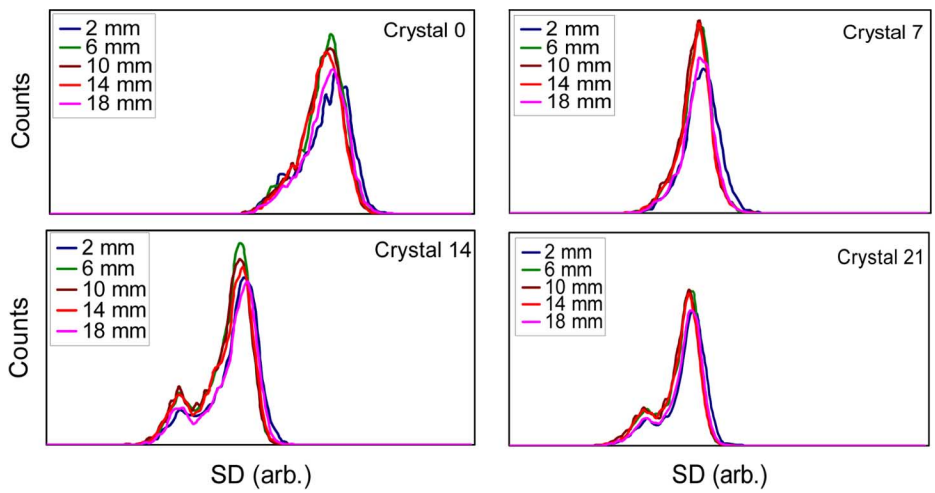

Fig. 5. Histograms of the measured standard deviation (SD) of the PMT signals for 4 individual crystals in the polished array, irradiated at five depths of 2, 6, 10, 14, and 18 mm. The locations of the crystals in the array are shown in Fig. 1.

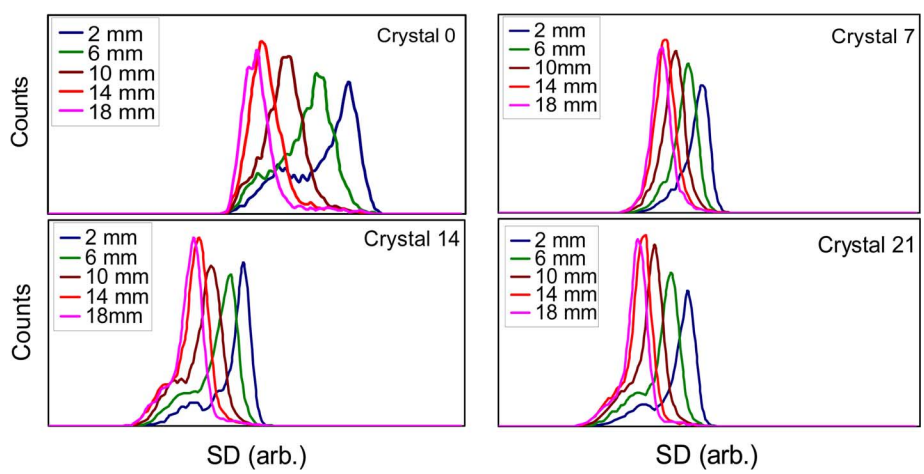

Fig. 6. Histograms of the measured standard deviation (SD) of the PMT signals for 4 individual crystals in the unpolished array, irradiated at five depths of 2, 6, 10, 14, and 18 mm. The locations of the crystals in the array are shown in Fig. 1.

in Fig. 4 for the three representative crystals. A lower energy threshold of 350 keV was applied, and no attempt was made to reject inter-crystal scatter events.

For the polished array, only a small difference in light distribution was observed at the three depths. A much larger change of the light distribution at the three depths was observed for the unpolished array. The amplitudes of the PMT channels farther from the crystal increased as the irradiation depth increased. For example, the amplitude of channel 15 increased 86% and 66% for crystals 0 and 14 respectively as the irradiation depth changed from 2 mm to 18 mm.

Fig. 5 shows histograms of the SD of the 16 PMT signals at five different depths for 4 crystals in the polished array. Little difference was observed for the SD values at the five depths. The DOI therefore cannot be measured for the polished array with this method. Fig. 6 shows histograms of the SD at 5 different depths for the unpolished array. The curves with the lowest SD correspond to a depth of 18 mm, where the light is distributed more uniformly across the PMT channels (giving lower SD) than for depths closer to the PMT. The change in SD is larger at depths closer to the PMT than at depths far from the PMT, therefore the DOI resolution is best close to the PMT. The small bumps at the left of the curves of crystals 14 and 21 shown in Fig. 5 and 6 are attributed to inter-crystal scatter events which have a more uniform light distribution because of their multiple interactions. The small bumps observed in the curves for crystal 0 at depths of 2 and 6 mm (Fig. 6) are contributed by the neighboring crystals due to crystal mis-identification. Fig. 7 shows the peak value of the SD histogram at five depths for the six crystals along the diagonal of the LSO array. The peak SD value was obtained using a Gaussian fit. The SD decreases linearly with increasing depth for small depths, with some flattening of the response above 15 mm. The absolute value of the SD primarily depends on the relative positions of the crystals on the PMT. The SD of crystal 0 and 35 is similar, as is crystal 7 and 28, and crystal 14 and 21. DOI calibration needs to be performed for each individual crystal to relate the measured SD to the DOI.

The calibration between SD and depth was accomplished by using a linear interpolation of the measured peak SD at depths of 2 and 18 mm for every individual crystal. After calibration, the horizontal axis on Fig. 6 can be converted to depth (mm). The resulting DOI distribution at each irradiation depth was fit

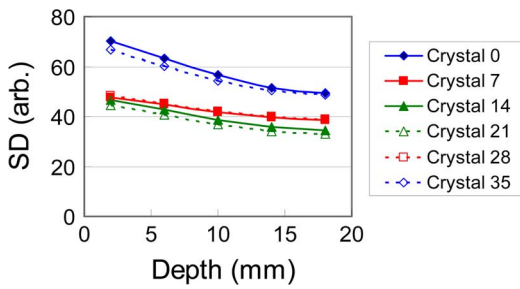

Fig. 7. The peak value of the standard deviation of 6 crystals from the unpolished array, irradiated at five depths of 2, 6, 10, 14, and 18 mm. The locations of the crystals in the array are shown in Fig. 1.

7.6	8.7	7.9	8.2	8.6	7.6
7.3	9.8	9.3	9.8	9.9	8.2
7.3	9.9	8.9	9.2	10.1	8.2
7.1	8.5	10.5	7.9	8.6	7.5
6.8	10.0	8.2	8.6	8.9	7.7
5.9	7.0	6.9	6.6	7.1	6.3

Fig. 8. DOI resolution measured for all 36 crystals in the unpolished array, averaged over all five depths.

TABLE I
PERCENTAGE OF EVENTS AT EACH OF 5 DEPTHS ASSIGNED TO TWO DOI BINS (0–10 AND 10–20 MM). THE RESULTS ARE THE AVERAGED OVER ALL CRYSTALS

Depth (mm)	2	6	10	14	18
Bin 1 (%)	9.0	19.1	52.1	87.0	93.1
Bin 2 (%)	91.0	80.9	47.9	13.0	6.9

with a Gaussian and the full width at half maximum (FWHM) used as a measure of the DOI resolution. The DOI resolution of all 36 crystals averaged across the five depths is shown in Fig. 8. In general the DOI resolution for crystals at the edge of the array was better than that of the crystals at the center of the array. The average FWHM DOI resolution was ~8 mm with a range of 5.9 to 10.5 mm. Table I shows the percentage of events that would be correctly assigned if the detector were split into two depth bins of 10 mm each. The stratification of events to two depth bins is very good, supporting the measured DOI resolution of 8 mm and demonstrating that this detector has a DOI performance that compares favorably with a two-layer phoswich detector. It was also observed that the DOI resolution of the bottom row of crystals was somewhat better than the top row of crystals. After further study, it was determined this was caused by slightly worse crystal identification for the top row of crystals compared with the bottom row of crystals. This is likely due to a combination of different coupling efficiency, non-uniformity in the MC-PMT photocathode, and the exact location of the LSO with respect to the MC-PMT pixel structure.

For the unpolished LSO array, no photopeak could be seen in the crystal energy spectra, because the light collection efficiency

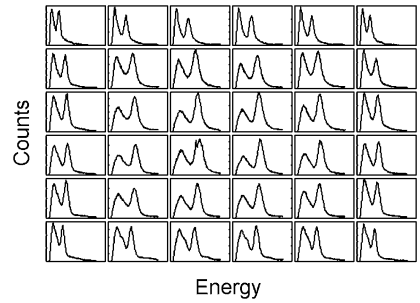

Fig. 9. Crystal energy spectra of all 36 crystals in the unpolished array after correction with the measured DOI.

is a strong function of depth. However, in this case, depth information is available that can be used to correct for this effect. The energy signal was corrected using the following equation:

$$E = E_0(1 + k \times D). \tag{3}$$

E and E_0 are the calibrated and measured energy respectively and D is the measured depth. k was estimated by fitting the measured photopeak positions averaged over all crystals at each of the five depths and was found to have a value of 0.05. The same value of k was applied to all crystals in the array. Fig. 9 shows the calibrated crystal energy spectra. A clear photopeak can now be seen and the average FWHM energy resolution is around 25% using a Gaussian fit of the photopeak.

IV. CONCLUSION

A new method of DOI encoding for a pixelated LSO array using a single multi-channel PMT was proposed and investigated. A polished LSO array and an unpolished LSO array were evaluated. The flood histogram of the polished array is better than that of the unpolished array, but no DOI information can be measured for the polished array with the proposed method. For the unpolished array the flood histogram is depth dependent, and all crystals can still be resolved for an LSO array of a crystal size of $1.3 \times 1.3 \times 20$ mm^3. An average DOI resolution of 8 mm (range 5.9–10.5 mm) was obtained, which is much worse than that measured with a dual-ended read out method (~3 mm) [36], but similar to that inherent in the use of a two-layer phoswich detector. However, the DOI resolution may be degraded when a larger array is used due to the increase in the fraction of multiple interaction events. A crystal energy resolution of 25% was obtained after the measured energy was corrected with the measured DOI. It has been shown by others that the SD of all channels of a multi-channel PMT can be obtained from an enhanced resistor network [31]. Therefore, only five signals (four signals to encode the x-y position and one signal to get the SD) need to be digitized for one multi-channel PMT. This is therefore an economical way to measure the DOI, as there is no photon detector in front of the LSO array and no need to use multiple layers of scintillator materials. To improve the DOI resolution, more work is required to optimize the detector, especially the reflector and surface treatments, to find the best compromise between flood histogram quality and DOI resolution.

REFERENCES

[1] S. Surti *et al.*, "Performance of philips gemini TF PET/CT scanner with special consideration for its time-of-flight imaging capabilities," *J. Nucl. Med.*, vol. 48, no. 3, pp. 471–480, Mar. 2007.

[2] G. Muehllehner and J. S. Karp, "Positron emission tomography," *Phys. Med. Biol.*, vol. 51, no. 13, pp. R117–R137, July 2006.

[3] D. W. Townsend, "Multimodality imaging of structure and function," *Phys. Med. Biol.*, vol. 53, pp. R1–R39, 2008.

[4] S. R. Cherry, "The 2006 Henry N. Wagner lecture: Of mice and men (and positrons)—Advances in PET imaging technology," *J. Nucl. Med.*, vol. 47, no. 11, pp. 1735–1745, Nov. 2006.

[5] S. R. Cherry, "Multimodality in vivo imaging systems: Twice the power or double the trouble?," *Annu. Rev. Biomed. Eng.*, vol. 8, pp. 35–62, 2006.

[6] T. K. Lewellen, "Recent developments in PET detector technology," *Phys. Med. Biol.*, vol. 53, pp. R287–R317, Aug. 2008.

[7] M. S. Judenhofer *et al.*, "Simultaneous PET-MRI: A new approach for functional and morphological imaging," *Nature Med.*, vol. 14, no. 4, pp. 459–465, Apr. 2008.

[8] C. Catana *et al.*, "Simultaneous acquisition of multislice PET and MR images: Initial results with a MR-compatible PET scanner," *J. Nucl. Med.*, vol. 47, no. 12, pp. 1968–1976, Dec. 2006.

[9] M. S. Judenhofer *et al.*, "PET/MR images acquired with a compact MR-compatiable PET detector in a 7-T magnet," *Radiology*, vol. 244, no. 3, pp. 807–814, Sept. 2007.

[10] C. Catana *et al.*, "Simultaneous in vivo positron emission tomography and magnetic resonance imaging," in *Proc. Nat. Acad. Sci. U.S.A.*, Mar. 2008, vol. 105, no. 10, pp. 3705–3710.

[11] H. Liang *et al.*, "A microPET/CT system for in vivo small animal imaging," *Phys. Med. Biol.*, vol. 52, no. 13, pp. 3881–3894, Jul. 2007.

[12] D. L. Prout, R. W. Silverman, and A. Chatziioannou, "Detector concept for OPET—A combined PET and optical imaging system," *IEEE Trans. Nucl. Sci.*, vol. 51, no. 3, pp. 752–756, Jun. 2004.

[13] Y. C. Tai *et al.*, "Performance evaluation of the microPET focus: A third-generation microPET scanner dedicated to animal imaging," *J. Nucl. Med.*, vol. 46, no. 3, pp. 455–463, Mar. 2005.

[14] Y. C. Tai *et al.*, "MicroPET II: Design, development and initial performance of an improved microPET scanner for small-animal imaging," *Phys. Med. Biol.*, vol. 48, no. 11, pp. 1519–1537, Jun. 2003.

[15] N. C. Rouze *et al.*, "Design of a small animal PET imaging system with 1 microliter volume resolution," *IEEE Trans. Nucl. Sci.*, vol. 51, no. 3, pp. 757–763, Jun. 2004.

[16] Y. Yang *et al.*, "Optimization and performance evaluation of the microPET II scanner for in vivo small-animal imaging," *Phys. Med. Biol.*, vol. 49, no. 12, pp. 2527–2545, Jun. 21, 2004.

[17] J. Seidel *et al.*, "Depth identification accuracy of a three layer phoswich PET detector module," *IEEE Trans. Nucl. Sci.*, vol. 46, no. 3, pp. 485–490, Jun. 1999.

[18] L. Eriksson *et al.*, "The ECAT HRRT: NEMA NEC evaluation of the HRRT system, the new high-resolution research tomograph," *IEEE Trans. Nucl. Sci.*, vol. 49, no. 5, pp. 2085–2088, Oct. 2002.

[19] N. Inadama *et al.*, "8-Layer DOI encoding of 3-dimensional crystal array," *IEEE Trans. Nucl. Sci.*, vol. 53, no. 5, pp. 2523–2528, Oct. 2006.

[20] K. Wienhard *et al.*, "The ECAT HRRT: Performance and first clinical application of the new high resolution research tomograph," *IEEE Trans. Nucl. Sci.*, vol. 49, no. 1, pp. 104–110, Feb. 2002.

[21] T. Tsuda *et al.*, "A four-layer depth of interaction detector block for small animal PET," *IEEE Trans. Nucl. Sci.*, vol. 51, no. 5, pp. 2537–2542, Oct. 2004.

[22] N. Orita *et al.*, "Three-dimensional array of scintillation crystals with proper reflector arrangement for a depth of interaction detector," *IEEE Trans. Nucl. Sci.*, vol. 52, no. 1, pp. 8–14, Feb. 2005.

[23] N. Zhang *et al.*, "A prototype modular detector design for high resolution positron emission mammography imaging," *IEEE Trans. Nucl. Sci.*, vol. 50, no. 5, pp. 1624–1629, Oct. 2003.

[24] P. A. Dokhale *et al.*, "Performance measurements of a depth-encoding PET detector module based on position-sensitive avalanche photodiode read-out," *Phys. Med. Biol.*, vol. 49, no. 18, pp. 4293–4304, Sep. 2004.

[25] J. S. Huber *et al.*, "Development of the LBNL positron emission mammography camera," *IEEE Trans. Nucl. Sci.*, vol. 50, no. 5, pp. 1650–1653, Oct. 2003.

[26] H. N. Du, Y. F. Yang, and S. R. Cherry, "Measurements of wavelength shifting (WLS) fibre readout for a highly multiplexed, depth-encoding PET detector," *Phys. Med. Biol.*, vol. 52, no. 9, pp. 2499–2514, May 2007.

[27] K. C. Burr *et al.*, "Evaluation of a prototype small animal PET detector with depth-of-interaction encoding," *IEEE Trans. Nucl. Sci.*, vol. 51, no. 4, pp. 1791–1798, Aug. 2004.

[28] K. Vetter, M. Burks, and L. Mihailescu, "Gamma-ray imaging with position-sensitive HPGe detectors," *Nucl. Instrum. Methods Phys. Res. A*, vol. A525, no. 1–2, pp. 322–327, Jun. 2004.

[29] E. A. Wulf *et al.*, "Germanium strip detector compton telescope using three-dimensional readout," *IEEE Trans. Nucl. Sci.*, vol. 50, no. 4, pp. 1182–1189, Aug. 2003.

[30] T. Ling, T. K. Lewellen, and R. S. Miyaoka, "Depth of interaction decoding of a continuous crystal detector module," *Phys. Med. Biol.*, vol. 52, no. 8, pp. 2213–2228, Apr. 2007.

[31] C. W. Lerche *et al.*, "Depth of gamma-ray interaction within continuous crystals from the width of its scintillation light-distribution," *IEEE Trans. Nucl. Sci.*, vol. 52, no. 3, pp. 560–572, Jun. 2005.

[32] Y. C. Wang *et al.*, "Performance evaluation of the GE healthcare eXplore VISTA dual-ring small-animal PET scanner," *J. Nucl. Med.*, vol. 47, no. 11, pp. 1891–1900, Nov. 2006.

[33] Y. F. Yang *et al.*, "A prototype PET scanner with DOI-encoding detectors," *J. Nucl. Med.*, vol. 49, no. 7, pp. 1132–1140, Jun. 2008.

[34] M. F. Weber *et al.*, "Giant birefringent optics in multilayer polymer mirrors," *Science*, vol. 287, no. 5462, pp. 2451–2456, Mar. 2000.

[35] J. R. Stickel, J. Y. Qi, and S. R. Cherry, "Fabrication and characterization of a 0.5-mm lutetium oxyorthosilicate detector array for high-resolution PET applications," *J. Nucl. Med.*, vol. 48, no. 1, pp. 115–121, Jan. 2007.

[36] Y. F. Yang *et al.*, "Depth of interaction resolution measurements for a high resolution PET detector using position sensitive avalanche photodiodes," *Phys. Med. Biol.*, vol. 51, no. 9, pp. 2131–2142, May 2006.

[37] M. S. Judenhofer, B. J. Pichler, and S. R. Cherry, "Evaluation of high performance data acquisition boards for simultaneous sampling of fast signals from PET detectors," *Phys. Med. Biol.*, vol. 50, pp. 29–44, 2005.